Ceramics International 51 (2025) 49676–49685

Contents lists available at ScienceDirect

Ceramics International

journal homepage: www.elsevier.com/locate/ceramint

Development of novel low-BaO based glass-ceramic glazes for porcelain stoneware tiles

Riccardo Fabris [a], Katarzyna Pasiut [b], Giulia Masi [a], Denia Mazzini [c], Giovanni Ridolfi [d], Paweł Rutkowski [b], Janusz Partyka [b], Maria Chiara Bignozzi [a,*]

[a] Department of Civil, Chemical, Environmental and Materials Engineering (DICAM) University of Bologna, via Terracini 28, 40131, Bologna, Italy
[b] AGH University of Science and Technology, Faculty of Materials Science and Ceramics, Department of Ceramic and Refractories, al. Mickiewicza 30, 30-059, Cracow, Poland
[c] Colorobbia Italia S.p.A., Via Bucciardi 37, Fiorano Modenese, Modena, 41042, Italy
[d] Centro Ceramico, Via Valle d'Aosta 1, Sassuolo, Modena, 41049, Italy

ARTICLE INFO

Handling Editor: Dr P. Vincenzini

Keywords:
BaO-Based glaze
Glass-ceramic glaze
Ceramic tile
Tribo-mechanical performance

ABSTRACT

In this study, novel glass-ceramic glazes are formulated for porcelain stoneware tiles to assess the impact of BaO concentration on their surface and aesthetic characteristics. The investigated glazes are within the Na_2O-K_2O-CaO-MgO-BaO-ZnO-Al_2O_3-SiO_2 system, with BaO content from 1.1 to 3.5 mol%. Unlike previous studies, this work provides a comprehensive assessment including Vickers microhardness, scratch resistance, and surface roughness, in addition to microstructural and thermal characterization. The results show that between 2.5 and 3.5 mol% BaO, glaze microstructure exhibits the coexistence of Na-anorthite and hyalophane crystals, while for 1.1 mol% BaO, (Ba, Na)-orthoclase and Na-anorthite are observed. Variations in crystalline phases, as well as in the amount of amorphous phase, significantly influence the final surface properties. The best performance in terms of Vickers microhardness, scratch resistance, surface roughness, and gloss is achieved for 2.5 mol% BaO and a crystalline content of 64 %.

1. Introduction

Porcelain stoneware tiles (PST) are defined as dense and largely vitrified ceramic materials that are characterised by remarkable physical, mechanical and technological properties [1,2]. Due to their high versatility, this typology of tiles is the most suitable for cladding indoor and outdoor surfaces [2–4]. To enhance their durability, PST are typically coated with a thin layer of glaze, which protects the underlying decoration against wear, scratches and impact [5–7]. Glaze coatings are defined as inorganic, non-metallic materials, whose chemical composition involves complex oxide systems obtained by mixing different raw materials (e.g., clays, feldspars, carbonates, etc.) and frits [8,9]. Typically, glaze formulations are designed within the framework of the Na_2O-K_2O-CaO-MgO-Al_2O_3-SiO_2 multi-component system [9,10]. By tailoring content and types of raw materials and frits as well as cooling conditions, two distinct types of glazes can be produced: amorphous and glass-ceramic glazes [5,11,12]. Amorphous glazes are usually characterised by high transparency and generally exhibit low tribological performances, thus limiting their use for ceramic tiles addressed to high-traffic areas. On the other hand, glass-ceramic glazes exhibit microstructures composed of polycrystalline phases embedded in an amorphous matrix thus increasing their tribomechanical performances and broadening their field of application [5,13–18]. The research on glass-ceramic glazes is still ongoing [5,13–18]. Several studies focused on the development of glass-ceramic glazes capable of crystallising anorthite ($CaAl_2Si_2O_8$) during firing [16–25]. Anorthite crystallisation allows the achievement of enhanced mechanical performances and satisfactory aesthetic appearance since the refractive index of anorthite is close to that of the amorphous matrix [17,23]. Wang et al. developed anorthite-based glass-ceramic glazes by mixing high-melting calcium frits with low-melting ones, obtaining a transparent glaze. They observed that the glaze with the highest content of crystalline structures exhibited the highest Vickers microhardness (8.1 GPa), and a matte appearance [17]. Additionally, Gajek et al. designed and characterised Ca- and Mg-based glass-ceramic glazes, finding that those with microstructures composed of diopside ($CaMgSi_2O_6$) and anorthite also exhibited high microhardness (HV = 8 GPa) [16].

Another approach recently adopted involves the incorporation of

* Corresponding author.
E-mail address: maria.bignozzi@unibo.it (M.C. Bignozzi).

https://doi.org/10.1016/j.ceramint.2025.08.207
Received 23 April 2025; Received in revised form 13 August 2025; Accepted 14 August 2025
Available online 15 August 2025

barium oxide (BaO) in the glaze formulations [13–15,26–31]. In particular, high concentrations of BaO enable the crystallisation of Ba-based aluminosilicate crystals, such as celsian ($BaAl_2Si_2O_8$) and hyalophane ($(K,Ba)Al_2Si_2O_8$) [13,27–30]. They usually increase the refractoriness of the final glaze and lead to a high refractive index that strongly reduces glaze transparency [26]. These studies [13,27–30] are mainly focused on examining the effects of BaO on the thermal and microstructural properties of glazes, without considering microhardness and scratch resistance. Only very recently, Pasiut et al. investigated the effect of BaO on glaze surface properties [31].

The aim of this study is to develop new formulations of Ba- and Ca-based glass-ceramic glazes with enhanced tribo-mechanical and aesthetic properties, such as matte finish and high transparency, while maintaining BaO content within the range of 1.1–3.5 mol%. To the best of our knowledge, no previous studies have explored the combination of low BaO content and detailed surface characterization. For this purpose, novel glaze formulations were designed, incorporating BaO and CaO up to 3.5 mol% and 9 mol%, respectively. The reported results are based on: (i) microstructural analysis of the coexistence of Ba- and Ca-based feldspar crystals; (ii) thermal characterization of the glazes; and (iii) investigation of correlations between microstructure and surface properties, including microhardness, scratch resistance, surface roughness, gloss, and colour variation.

2. Materials and methods

2.1. Materials

Four different commercial frits, designated IF-1 to IF-4, were kindly supplied by Colorobbia Italia S.p.a. (Fiorano Modenese, Modena, Italy). The chemical composition of the selected frits, determined using X-ray fluorescence spectroscopy (XRF, Axios Max, PANalytical), is reported in Table 1. Quartz (SiO_2), spodumene ($LiAlSi_2O_6$), nepheline ($KNa_3[AlSiO_4]_4$), kaolin ($Al_2Si_2O_5(OH)_4$) and K-feldspar ($KAlSi_3O_8$), kindly supplied by Colorobbia Italia (Fiorano Modenese, Modena, Italy), were also used as raw materials for glaze preparation.

2.2. Glazes and samples preparation

Four glass-ceramic glazes (named GST-1, GST-2, GST-3 and GST-4), based on the Na_2O-K_2O-CaO-MgO-BaO-ZnO-Al_2O_3-SiO_2 multi-component system, were prepared by mixing the commercial frits IF-1, IF-2, IF-3 and IF-4 with raw materials as reported in Table 2. While the composition of the different frits varies significantly in the investigated glazes, the amounts of raw materials were intentionally adjusted to minimize variations. In particular, the spodumene content was maintained within the 4.6–5.0 wt% range. This amount is considered sufficient—based on industrial experience—to produce glazes with good chemical resistance, thermal stability and reasonable cost. A detailed investigation of the effects of higher amounts of spodumene falls outside the scope of the present study.

A 500 g glaze batch was wet-milled for 50 min in a ceramic jar with 500 g of alumina balls, 40 wt% water, and 0.3 wt% carboxymethylcellulose (CMC). The resulting slurry was then sieved using a 200-mesh sieve to remove coarser particles. The density of the slurry was measured using a 100 mL pycnometer and adjusted to 1450 kg/m^3 by adding water. The chemical composition of the investigated glazed measured by XRF is reported in Table 3.

Table 2
Amount (wt%) of industrial frits and raw materials for the investigated glazes.

Typology	Name	GST-1	GST-2	GST-3	GST-4
Industrial Frits	IF-1	25.0	25.0	22.0	22.0
	IF-2	25.0	–	12.0	12.0
	IF-3	–	25.0	22.0	16.0
	IF-4	–	–	–	6.0
Raw materials	Quartz	2.9	2.9	2.7	2.7
	Spodumene	5.0	5.0	4.6	4.6
	Nepheline	25.1	25.1	22.8	22.8
	Kaolin	7.1	7.1	5.5	5.5
	K-feldspar	9.9	9.9	8.4	8.4

Each slurry was applied using the airless technique onto 30 cm × 30 cm unfired porcelain stoneware bodies in the amount of 44 mg/cm^2. The unfired bodies were previously prepared by pressing spray-dried powders (kindly supplied by Meta S.p.A., Italy) at 34.3 MPa. For each glaze formulation, a 30 cm × 30 cm sample was prepared, dried for 1 h in an electric ventilated oven, and then single-fired in an industrial roller kiln. A fast-firing cycle was employed with the following parameters: a heating rate of 30 °C/min, a peak temperature (T_P) of 1205 °C held for 5 min, and a cooling rate of approximately 200 °C/min.

These samples were used for scanning electron microscopy analysis and for the determination of Vickers microhardness, scratch resistance, gloss, and surface roughness.

To evaluate glaze transparency, each glaze was applied onto ceramic tiles decorated with white and black plain-coloured patterns, printed using an inkjet digital printer (Digiglaze, System, Italy) with a four-color process based as follows: Cyano: IKTP 01003, Brown: IKTP 06004, Honey: IKDP 02009.

BLACK: IKTP 04008). The glazed tiles were then fired under the same conditions previously described. Additionally, two unglazed decorated tiles—one fully white and one fully black—were prepared as reference samples.

For X-ray diffraction (XRD) analysis, glaze samples were prepared as follows: the glaze slurry was dried, milled, and sieved to obtain a particle size smaller than 0.063 mm. Approximately 5 g of glaze powder was then pressed using a hydraulic press (P = 2 MPa) to form a 25 mm diameter glaze disc. For each glaze, two discs were prepared and fired under the same conditions used for the glazed tiles.

2.3. Samples characterisation

Microstructural analyses were carried out using a FEG-SEM (Scios 2 Dual Beam, Thermo Scientific) equipped with an energy-dispersive X-ray spectroscopy detector (EDS, EDAX Octane Elite, Ametek). Investigations were carried out on the glazed surface of 10 cm × 10 mm samples cut from 30 × 30 cm ceramic tiles. Observations were performed before and after etching sample surfaces with 40 % (v/v) hydrofluoric acid (HF, Chempur, Piekary Śląskie, Poland) for 30 s. Such a high HF concentration was selected based on multiple trials. Given its high reactivity, the HF solution was applied to the sample surface for a limited time (i.e., 30 s).

After etching, samples were rinsed with distilled water and then

Table 1
Chemical composition (mol%) of industrial frits (IF). R_2O/RO molar ratios are reported according to the Herman Seger's method ($R_2O = Na_2O + K_2O$ and RO = CaO + MgO + BaO + ZnO).

Name	Na2O	K2O	CaO	MgO	BaO	ZnO	Al2O3	B2O3	SiO2	R2O/RO
IF-1	4.4	0.7	16.9	1.7	–	1.7	18.6	1.0	55.2	0.25
IF-2	5.1	0.8	1.4	4.0	15.6	2.9	11.7	–	58.4	0.25
IF-3	3.3	2.2	17.2	–	4.5	7.6	6.8	2.0	56.3	0.19
IF-4	–	0.7	25.2	13.7	–	–	11.4	–	49.0	0.02

Table 3
Chemical composition (mol%) by XRF of the investigated glazes. SiO_2/Al_2O_3 and Na_2O/K_2O molar ratios are also reported. R_2O/RO molar ratios are reported according to the Herman Seger's method ($R_2O = Na_2O + K_2O + Li_2O$ and $RO = CaO + MgO + BaO + ZnO$). Li_2O was below the detection limit by XRF (i.e. 1 wt%), thus it was estimated based on the amount of Li_2O (≈6 wt %) provided by spodumene.

Name	Na_2O	K_2O	Li_2O[a)]	CaO	MgO	BaO	ZnO	Al_2O_3	SiO_2	SiO_2/Al_2O_3	Na_2O/K_2O	R_2O/RO
GST-1	5.3	2.5	0.7	5.0	1.4	3.5	1.1	15.3	65.1	4.3	2.1	0.77
GST-2	4.8	2.8	0.7	9.0	0.5	1.1	2.3	14.0	64.4	4.6	1.7	0.64
GST-3	4.8	2.6	0.7	8.1	0.8	2.7	2.4	13.7	63.7	4.6	1.8	0.58
GST-4	4.7	2.5	0.7	8.6	1.7	2.5	1.9	14.0	63.2	4.5	1.9	0.54

[a)] Li_2O content in spodumene was about 6 wt%. Considering spodumene addition in the glaze mixes as reported in Table 2, Li_2O content is estimated to be 0.3 wt%, equivalent to 0.7 mol%.

ultrasonically cleaned for 1 h to remove any residue. Samples were made conductive by applying a thin layer of graphite using a high-vacuum sputter coater (EM ACE 600, Leica Microsystems). Micrographs were acquired under low-vacuum conditions using backscattered electrons, with a working distance of 8.5 mm and an electron beam voltage of 15 kV.

Glaze mineralogical composition was investigated using an X-ray diffractometer (XRD, X'Pert PANalytical Pro, Malvern PANalytical) equipped with an X-ray source emitting Cu-Kα radiation (λ = 1.5405 Å) and a detector (PIXcel1D, Malvern PANalytical). XRD spectra were acquired in the 2θ range from 10° to 80°, with a step size of 0.016° and a scanning rate of 0.01°/s. Measurements were performed on powders obtained by milling and sieving (fraction smaller than 0.063 mm) fired glaze disk samples. Crystalline phase identification was carried out by comparing the acquired spectra with ICDD (International Centre for Diffraction Data) reference patterns, while phase quantification was performed using the Rietveld refinement method. Samples for quantitative analysis were prepared by adding 5 wt% high-purity zinc oxide (99.9 % ZnO, Sigma-Aldrich) to 5 g of glaze powder. Qualitative and quantitative analyses were performed using HighScore Plus.

Glaze characteristic temperatures were measured using a hot-stage microscope (HSM, Misura 3 HSM 1600, Expert System Solutions Srl). This thermal analysis was performed at 10 °C/min on a cylindrical pellet (d = 2 mm, h = 3 mm) made with unfired glaze powder properly prepared. Glaze characteristic temperatures, such as sintering (T_S), softening (T_{SO}), sphere (T_{SH}), hemisphere (T_{ESH}), and melting (T_M) temperatures, were acquired using dedicated software (Misura 3.32, Expert System Solutions Srl).

Glass transition temperature (Tg) and the onset of crystallisation were determined by differential thermal analysis (DTA, STA 409 CD, Netzsch). Measurements were performed by placing 110 ± 5 mg of unfired glaze powder (fraction smaller than 0.063 mm), into platinum crucible with a heating rate of 10 °C/min, from room temperature (≈25 °C) up to 1205 °C (T_P).

Glaze viscosity (η) was estimated by the Vogel - Fulcher - Tammann (VFT) equation (Eq. (1)) where A, B, and T_0 are constants [10]:

$$\text{Log } \eta = A + (B/T\text{-}T_0) \quad (1)$$

This equation was solved considering the three known viscosity values of $10^{12.5}$ Pa s, $10^{6.3}$ Pa s, and $10^{5.4}$ Pa s in correspondence to T_g, T_{SO} and T_{ESH}, respectively [32–34].

The coefficient of thermal expansion (CTE) was measured using a mechanical dilatometer (DIL 402C, Netzsch). Measurements were carried out at a heating rate of 10 °C/min on bulk cylindrical bars (d = 5 mm, h = 50 mm), prepared by rolling highly plastic glaze slurries, which were then dried and fast-fired.

Vickers microhardness (HV) measurements were carried out on the mirror-like polished cross-section of 10 mm × 10 mm sample, obtained by cutting 30 cm × 30 cm ceramic tile. Indentation was performed along the glaze layer using an automatic microhardness indenter (Galileo ISOSCAN CN03+, LTF Spa Industry). For each sample, at least 5 indentations were made with a load of 9.81 N and a dwell time of 15 s according to ASTM C1327-15 [35]. After each indentation, the diagonals were measured by using dedicated image analysis software (ISOSCAN, LTF Spa Industry).

Scratch resistance tests were performed by sliding different Mohs minerals across the surface of 15 cm × 15 cm specimens obtained by cutting from 30 cm × 30 cm ceramic tile, following the procedure reported in ISO 6769:2022 [36].

The average roughness (Ra) and the maximum height of the roughness profile (Rz) were measured using a confocal laser scanning microscope (CLSM, Lext OLS4000, Olympus). For each sample, two 3D areas (2560 μm × 2560 μm) were measured using a 5X confocal objective. Measurements were carried out on 5 cm × 5 cm samples previously used for gloss assessment. Finally, the Ra and Rz values were calculated by extracting twelve profiles from each measured area according to ISO 21920-2 [37].

Gloss measurements were performed on the surface of 5 cm × 5 cm sample cut from 30 cm × 30 cm ceramic tile using a glossmeter (Elcometer 406L, Elcometer). For each sample, five measurements were carried out using a 60° probe.

Glaze coating transparency was evaluated by calculating colour variation (ΔE*) using Equation (2), where ΔL*, Δa*, and Δb* represent the variation in colour coordinates between UG and glazed PST [38].

$$\Delta E^* = ((\Delta L^*)^2 + (\Delta a^*)^2 + (\Delta b^*)^2)^{(1/2)} \quad (2)$$

Colour coordinates were measured using a portable colorimeter (NH310, Zetalab srl) equipped with a D65 LED illuminant and a measurement aperture of 8 mm. For each coloured area, twenty measurements were taken.

3. Results and discussion

The microstructures of glazes GST-1, GST-2, GST-3, and GST-4 were initially investigated by SEM and XRD analyses. Micrographs of glazed samples before and after HF etching are shown in Fig. 1.

Observations of the unetched surfaces reveal that all the samples exhibit high-brightness crystalline clusters, which are partially covered by a thin glassy layer, hindering a clear identification of crystal morphology. For this reason, samples were also examined after HF etching, which preferentially dissolves the thin glassy layer due to its higher corrosion rate compared to crystalline structures [39–41]. After etching, the micrographs reveal the presence of micro-cavities and crests, resulting from the selective dissolution induced by HF. Micrographs of GST-1, GST-3, and GST-4 highlight the coexistence of two distinct types of crystalline clusters: low-brightness needle-like clusters and high-brightness clusters with square and bar-shaped morphologies. GST-2 exhibits a microstructure composed of low-brightness needle-like crystals evenly distributed across the observed area, with medium-brightness square-shaped crystals appearing sporadically as isolated spots. Furthermore, while GST-1 is characterised by fine crystals with dimensions smaller than 5 μm, GST-2, GST-3, and GST-4 feature larger crystals ranging from 5 to 10 μm. To assess the chemical composition of both crystalline structures and amorphous phases, EDS analysis was performed on the etched surface. The EDS spectra are shown in Fig. 2.

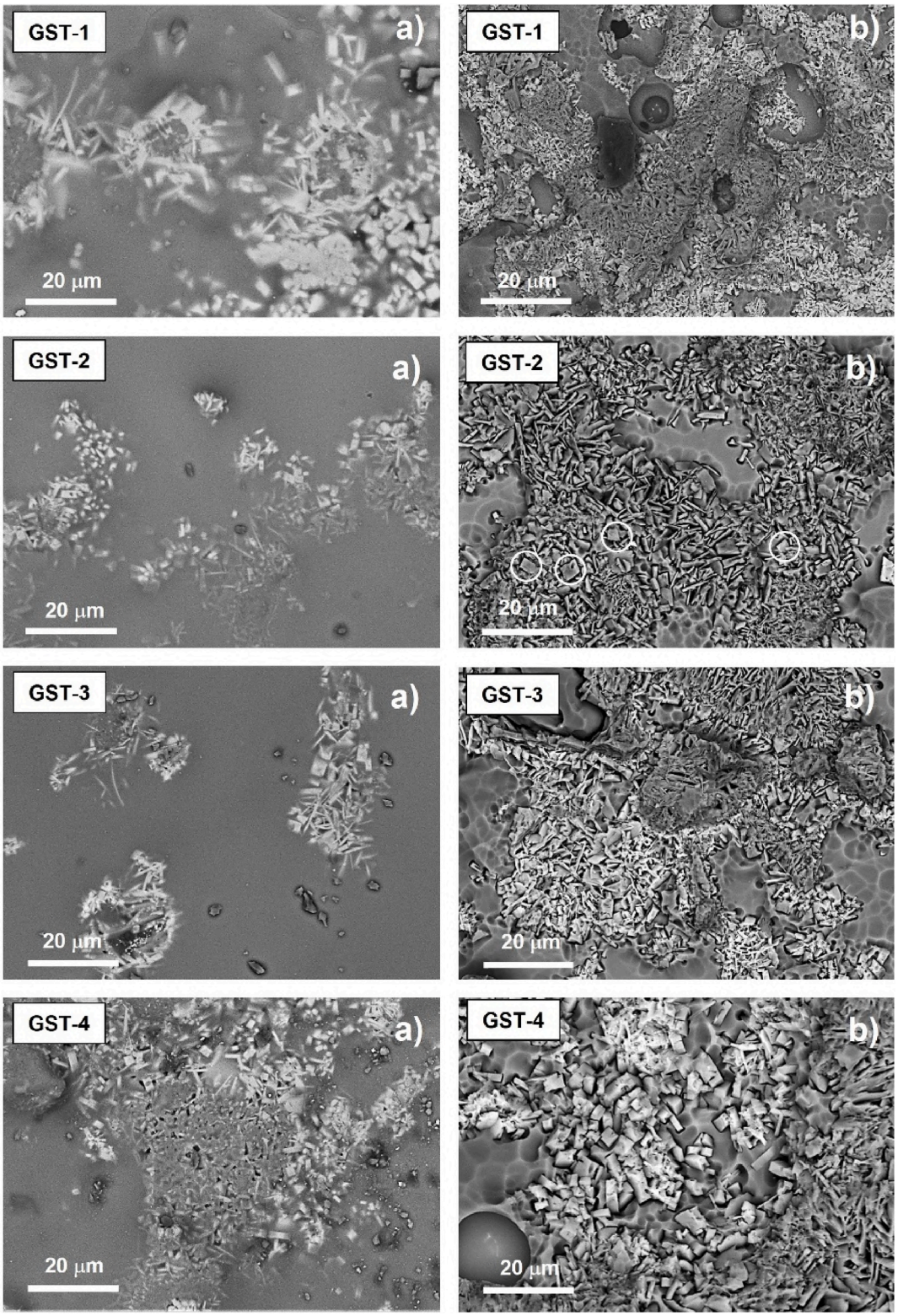

Fig. 1. Microstructural observations acquired by backscattered electron (BSE) performed on glaze surfaces: a) before and b) after HF etching. In GST-2 (image b), medium-brightness, square-shaped crystalline phases are circled in white.

The EDS analysis of the low-brightness needle-like crystals reveals high concentrations of Ca, Si, and Al, indicating that they are Ca-based aluminosilicate crystals (Fig. 2, area A2, A5, A8 and A11). Conversely, the chemical composition of the square- and bar-shaped crystals exhibits high concentrations of Ba, Si, and Al, identifying them as Ba-based aluminosilicate crystals (Fig. 2, area A3, A9 and A12). Additionally, peaks of Na and K suggest that these structures can be solid solutions, respectively belonging to the plagioclase and hyalophane feldspar series. Large angular grains composed of Si and O were locally detected (Fig. 2, A6), probably representing quartz crystals. Furthermore, EDS spectra of the amorphous matrix (Fig. 2, area A1, A4, A7 and A10) highlight traces of Ba in all the analysed samples.

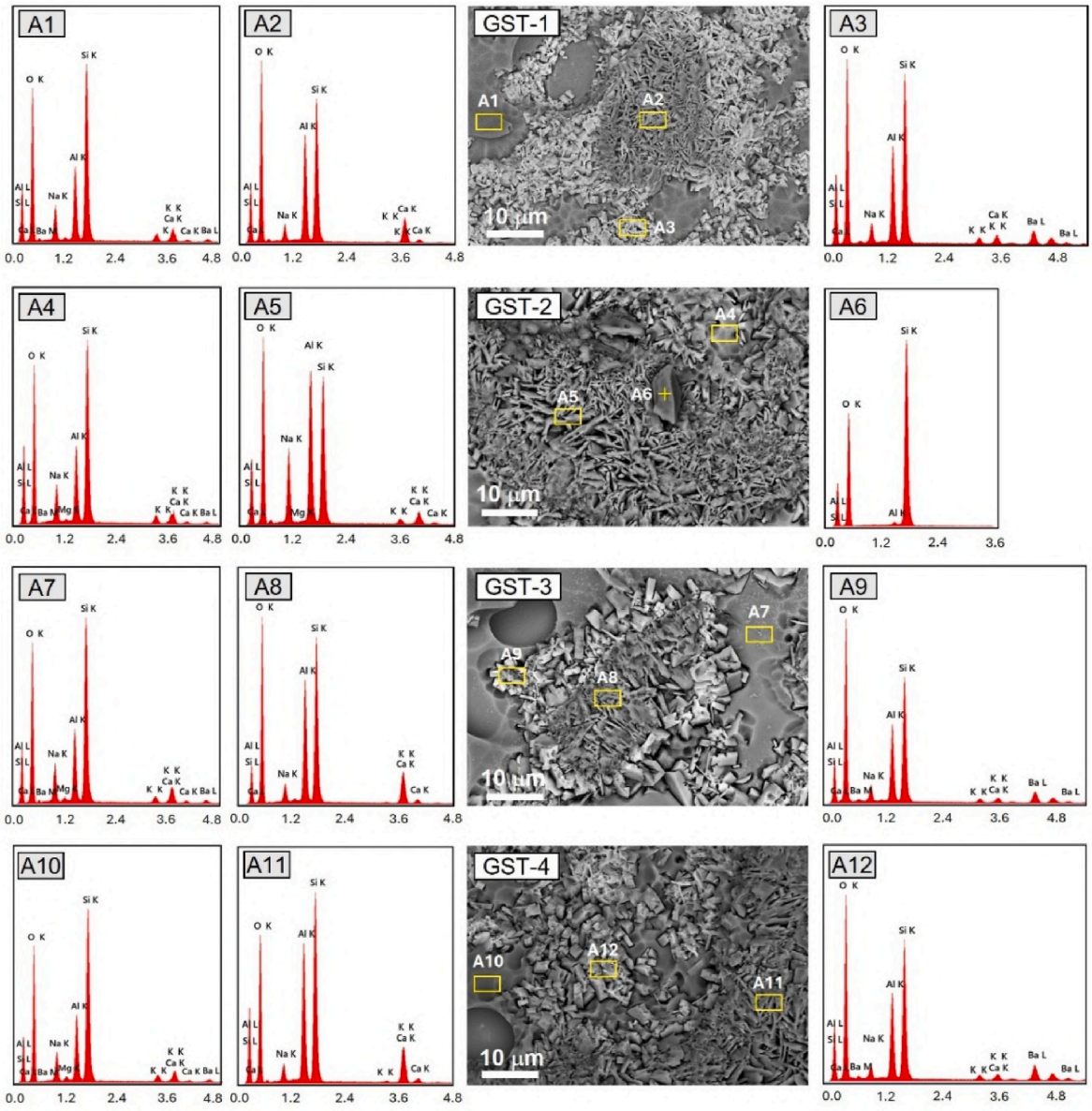

Fig. 2. EDS analysis on different areas of GST-1, GST-2, GST-3 and GST-4.

To identify the nature of the different crystalline structures observed by SEM, XRD analysis was carried out and the spectra are reported in Fig. 3.

Quartz (ICDD 98-008-3849) was always detected, and its presence is mainly attributed to incomplete dissolution during the fast-firing cycle, characterised by a high heating rate and a short dwell time at peak temperature. Quartz was used as a raw material in the glaze formulations (2.5–3 wt%) and may also be present as an impurity in kaolin and feldspar raw materials [22]. The presence of Na-anorthite ($Ca_{0.54}Na_{0.48}Al_{1.52}Si_{2.48}O_8$, ICDD: 98-002-9361) was also detected in all the analysed samples. This phase corresponds to an intermediate solid solution belonging to the plagioclase series, characterised by albite ($NaAlSi_3O_8$) and anorthite ($CaAl_2Si_2O_8$) as end members [22]. It has been reported in the literature that anorthite is typically in the form of needle or flake-like crystals [5,17,22,23] as observed in Fig. 2 (areas A2, A5, A8, A11). Hyalophane ($K_{0.47}Ba_{0.4}Na_{0.13}Al_{1.41}Si_{2.6}O_8$, ICDD: 98-003-1192) was detected in GST-1, GST-3, and GST-4. This crystalline phase is a solid solution between orthoclase ($KAlSi_3O_8$), celsian ($BaAl_2Si_2O_8$) and occasionally albite, and belongs to the feldspar crystals group [27,28,42].

The presence of Na^+ in this crystalline phase may be attributed to an incomplete ion exchange reaction between crystals and the surrounding matrix [42]. This phase has been associated with the high-brightness bar- and square-shaped crystalline structures shown in Fig. 2, based on the EDS results for areas A3, A9, and A12. In GST-2, the presence of (Ba, Na)-orthoclase ($Ba_{0.19}Na_{0.22}K_{0.59}Al_{1.18}Si_{2.82}O_8$ ICSD: 98-010-0182), corresponding to a solid feldspar solution like that of hyalophane but with a lower amount of celsian compared to albite and orthoclase, was revealed. (Ba, Na)-orthoclase corresponds to the medium-brightness square-shaped crystals sporadically observed in Fig. 1 (white circled area in GST-2 (b)). The detection of (Ba, Na)-orthoclase is in accordance with the lower amount of BaO present in GST-2 formulation compared to the other investigated glazes. To the best of our knowledge, the crystallisation of (Ba, Na)-orthoclase at a low BaO concentration (1.1 mol%) has not previously been reported in the literature. Gajek et al., in a study on glass–ceramic glazes developed within the K_2O-MgO-CaO-BaO-Al_2O_3-SiO_2 system, observed that BaO concentrations below 1 mol% contribute exclusively to the formation of amorphous phases [26].

Finally, both hyalophane and (Ba, Na)-orthoclase are solid solutions

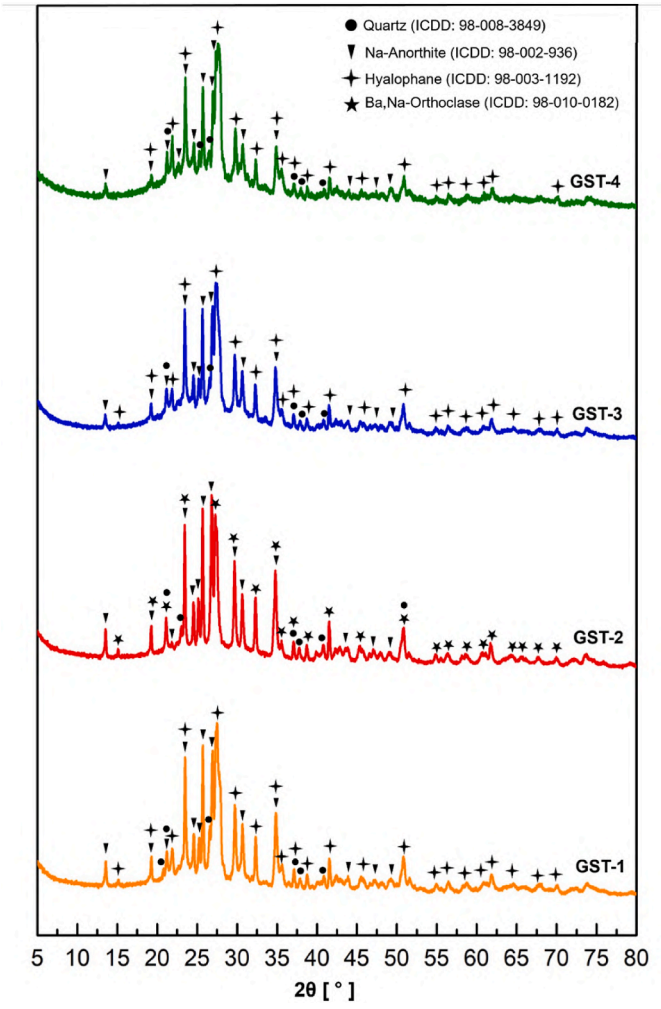

Fig. 3. XRD patterns of GST-1, GST-2, GST-3 and GST-4.

characterised by a disordered crystalline lattice. Specifically, Pasiut et al. investigated the nature of hyalophane crystalline structures, highlighting that this crystal can crystallise in both monoclinic and triclinic systems with various order-disorder degrees [31]. According to the obtained data, both (Ba, Na)-orthoclase and hyalophane are characterised by a monoclinic crystalline lattice like that of orthoclase. However, due to the reduced amount of Ba^{2+} and Na^{+} cations participating, (Ba, Na)-orthoclase exhibits a lower degree of disorder and a lattice closer to orthoclase compared to hyalophane. Quantitative analysis of the main phases was determined by the Rietveld refinement method, and the results are presented in Table 4. In Table 5, crystalline and amorphous content in the glazes have also been reported expressed both in volume and weight percentages.

GST-1 and GST-2 exhibit the highest and the lowest degrees of crystallinity, respectively. In all the analysed glazes, the crystalline content exceeds 50 wt%. Moreover, the results indicate that Na-anorthite is the most abundant phase, while the hyalophane content progressively decreases in GST-1, GST-3, and GST-4 as the BaO content

Table 4
Quantitative phase analyses of GST glazes by Rietveld refinement method.

Phases	GST-1	GST-2	GST-3	GST-4
Na-anorthite (wt%)	37.9	39.2	33.0	40.3
Hyalophane (wt%)	32.3	–	25.8	23.6
(Ba, Na)-orthoclase (wt%)	–	11.7	–	–
Amorphous phase (wt%)	29.8	49.1	41.2	36.1

Table 5
Crystalline and amorphous content in the glazes (wt% and vol%).

	Crystalline content [(a)] (wt%)	Amorphous content [(a)] (wt%)	Crystalline content [(b)] (vol%)	Amorphous content [(b)] (vol%)	Density (g/cm^3) [(c)]
GST-1	70.2	29.8	77.3	22.7	2.99
GST-2	50.9	49.1	55.3	44.7	2.92
GST-3	58.8	41.2	64.3	35.7	2.97
GST-4	63.9	36.1	70.0	30.0	2.98

[(a)] Determined by Rietveld refinement.
[(b)] Calculated using glaze density values and $d_{Na\text{-}anorthite} = 2.73\ g/cm^3$, $d_{Hyalophane} = 2.70\ g/cm^3$, $d_{(Ba,\ Na)\text{-}orthoclase} = 2.56\ g/cm^3$).
[(c)] Calculated based on the chemical compositions reported in Table 3.

in the glaze formulation decreases. Notably, only GST-2 exhibits (Ba, Na)-orthoclase, consistent with the presence of 1.1 mol% BaO.

Glaze characteristic temperatures were determined by DTA and HSM and are collectively presented in Table 6.

All the analysed glazes exhibit very similar Tg values, ranging from 628.6 to 635.1 °C, suggesting that their molecular mobility begins at approximately the same temperature. Similarly, glaze crystallisation temperatures fall within a narrow range (905.3 ÷ 912.8 °C) and can be attributed to the crystallisation of Na-anorthite, (Ba, Na)-orthoclase and hyalophane crystals, previously identified by XRD. According to the literature, crystallisation peaks of Ca- and Ba-based aluminosilicate feldspar crystals are found at a very similar temperatures [13,17,23]. The results of HSM reveal that GST-1 exhibits the highest characteristic temperatures (T_S, T_{SO}, T_{SH}, T_{ESH}), making it the most refractory glaze, while GST-2 and GST-3 are both highly fusible. GST-4 exhibits the best thermal performance during the firing cycle, with its softening phase occurring at the peak temperature of the process (T_P = 1205 °C).

Glaze viscosity was estimated using Eq. (1), and the logarithmic viscosity-temperature curves (log(η)-T) are shown in Fig. 4. As expected, the curves show an inverse relationship between log(η) and temperature. The log(η)-T curves for GST-1 and GST-2 show the slowest and fastest decreases, respectively, thereby exhibiting the highest and the lowest η values at T_P, and thus differently influencing the densification process during firing. GST-3 and GST-4 show η values at T_P comparable to that observed for GST-2.

The high viscosity and low fusibility of GST-1 can thus be attributed to its high BaO content, which acts as a high-temperature fluxing agent, as well as the low content of CaO and ZnO, which act as medium- and low-temperature fluxing agents, respectively [13,23]. In fact, during firing the high BaO content in GST-1 leads to an increased number of Ba^{2+} cations in the glaze matrix. Due to their large ionic radius (r = 1.46 Å), these cations hinder the movement of smaller ones, reducing ionic mobility and consequently increasing glaze viscosity [39,43]. Therefore,

Table 6
Characteristic temperatures of GST glazes measured at 10 °C/min, determined by DTA and HSM. Tg, Tc, T_S, T_{SO}, T_{SH}, T_{ESH}, and T_M correspond to the glass transition, crystallisation, sintering, softening, sphere, hemisphere, and melting temperatures.

Samples	DTA		Hot stage microscope				
	Tg	Tc	T_S	T_{SO}	T_{SH}	T_{ESH}	T_M
	[°C]	[°C]	[°C]	[°C]	[°C]	[°C]	[°C]
GST-1	634.1	912.8	1160	1225	1257	1266	1315
GST-2	628.6	909.7	1112	1155	1197	1245	1273
GST-3	634.7	905.3	1120	1168	1197	1209	1220
GST-4	635.1	908.8	1134	1180	1215	1220	1263

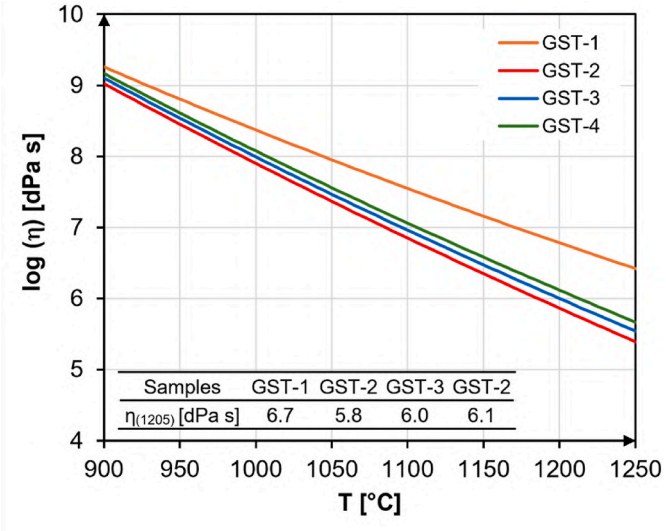

Fig. 4. Logarithmic viscosity-temperature curves (log(η)-T) for GST-1, GST-2, GST-3 and GST-4.

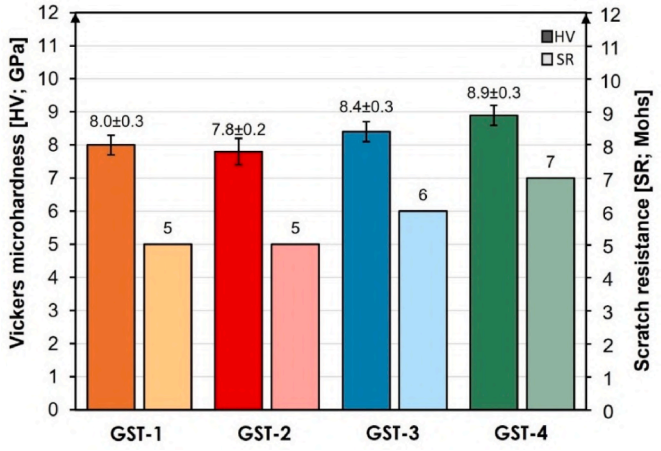

Fig. 5. Results of HV and SR measurements.

the high viscosity and refractoriness of GST-1 affect the glaze microstructure, thereby hindering crystal growth and leading to the formation of very fine crystals, as observed in Fig. 1b. Additionally, the nucleation of a higher number of crystalline phases as for GST-1 (Tables 4 and 5) leads to an increase in glaze viscosity [13,14,44]. In contrast, for GST-2, GST-3, and GST-4 (Fig. 1b), the high fusibility and low viscosity facilitate the growth of crystalline phases, resulting in a crystalline structure with larger grain sizes. Moreover, for GST-2, it is possible that the combination of the lowest viscosity at T_P and the lowest amount of BaO (1.1 mol%) creates the conditions for the nucleation of only (Ba, Na)-orthoclase. Further investigations are currently underway on this aspect with glazes specifically formulated with BaO contents ranging from 0.5 to 1.5 mol%.

Another factor influencing the durability of glaze is the coefficient of thermal expansion (CTE). Its evaluation is crucial for assessing the compatibility between the glaze and the ceramic body; an excessive mismatch between thermal expansion values may lead to structural defects, such as cracking, crazing, or glaze detachment, ultimately compromising the performance of glazed ceramic tiles. The CTE values of the investigated glaze are presented in Table 7. GST-3 and GST-4 exhibit the lowest CTE values, while GST-2 has the highest ($CTE_{GST\text{-}3} \approx CTE_{GST\text{-}4} < CTE_{GST\text{-}1} < CTE_{GST\text{-}2}$). Additionally, a comparison of these values with that of the porcelain stoneware body ($CTE_{PST\ body} = 77.0 \times 10^{-7}$) highlights that the latter is slightly higher than the GST ones ($CTE_{PST\ body} > CTE_{GST}$).

This suggests that during cooling, the glaze layer promotes a slight compressive stress state due to the higher coefficient of thermal expansion (CTE) of the ceramic body, which enhances its mechanical performance and resistance to impact and thermal shock.

Both the microstructural and thermal characteristics of glazes influence their tribomechanical performance, making their evaluation crucial for assessing their suitability for specific applications [14,15]. Therefore, Vickers microhardness (HV) and scratch resistance (SR) were measured on the investigated glazes, and the results are reported in Fig. 5.

GST-1 and GST-2 exhibit the lowest HV and SR values, despite the former showing the highest degree of crystallisation. Their low tribomechanical performance is somewhat expected, as it is strongly related to the presence of BaO, which is added at the highest and lowest concentrations, respectively. In fact, as previously observed, GST-1 exhibits the highest refractoriness and viscosity, which leads to incomplete densification and, consequently, poor surface properties. In contrast, GST-2 shows the lowest content of crystalline phases (Na-anorthite and a low degree of crystallisation of (Ba, Na)-orthoclase crystals), due to the lowest BaO content in the formulation. The HV for GST-2 is comparable to those of anorthite-based glass-ceramic glazes [16,17]. Conversely, GST-3 and GST-4 display the highest HV and SR values, which can be primarily ascribed to microstructures characterised by extensive networks of hyalophane and Na-anorthite, surrounded by a lower amount of amorphous phase compared to GST-2. It is well established in the literature that the coexistence of different crystalline structures generally leads to an improvement in the mechanical performance of glazes [16]. Furthermore, the presence of BaO in the amorphous phase (as detected by EDS in areas A1, A4, A7, and A10 of Fig. 2) also contributes to the increase in HV, as demonstrated in BaO-based glass by Zakaly et al. [45].

Another important parameter for glazes is their surface finish. To assess this, three-dimensional surface maps (Fig. 6) were acquired, and the Ra and Rz roughness parameters were measured (Fig. 7). The values of these parameters increase with the glaze crystallinity content, as reported in the literature [10,31,46]. Specifically, GST-1 and GST-4 exhibit complex textures with surface irregularities homogeneously distributed across the analysed areas (Fig. 6), and they show the highest Ra and Rz values. In contrast, GST-2 and GST-3 display smoother surfaces and lower Ra and Rz values, consistent with their lower crystalline content.

The aesthetic appearance and surface finish of glazes are fundamental aspects to consider in the production of high-quality ceramic tiles. Therefore, gloss values (G) and colour change (ΔE*) were also evaluated. The results of gloss measurements, reported in Fig. 8 show the following trend: $G_{GST\text{-}1} \sim G_{GST\text{-}4} < G_{GST\text{-}3} < G_{GST\text{-}2}$. GST-1 and GST-4 exhibit the lowest gloss values equal to 4.5 and 5.4, respectively, corresponding to a matte surface. Since gloss is negatively influenced by light scattering caused by crystalline structures embedded in the glaze amorphous phase, these results are in good agreement with the high crystalline phase content (70 and 64 wt% corresponding to 77 and 70 vol%, respectively) determined for GST-1 and GST-4. Furthermore, the literature suggests that the presence of Ba-based crystals contributes to gloss reduction, mainly due to the high molecular weight of BaO [13,30,31].

Finally, the transparency of the investigated glazes was evaluated by assessing the colour change (ΔE*) on full-colour white and black ceramic tiles. Colorimetric coordinates were measured before and after

Table 7
CTE value for both PST body and GST glazes.

Samples	GST-1	GST-2	GST-3	GST-4
CTE [°C^{-1}]	66.3×10^{-7}	70.7×10^{-7}	64.1×10^{-7}	64.3×10^{-7}

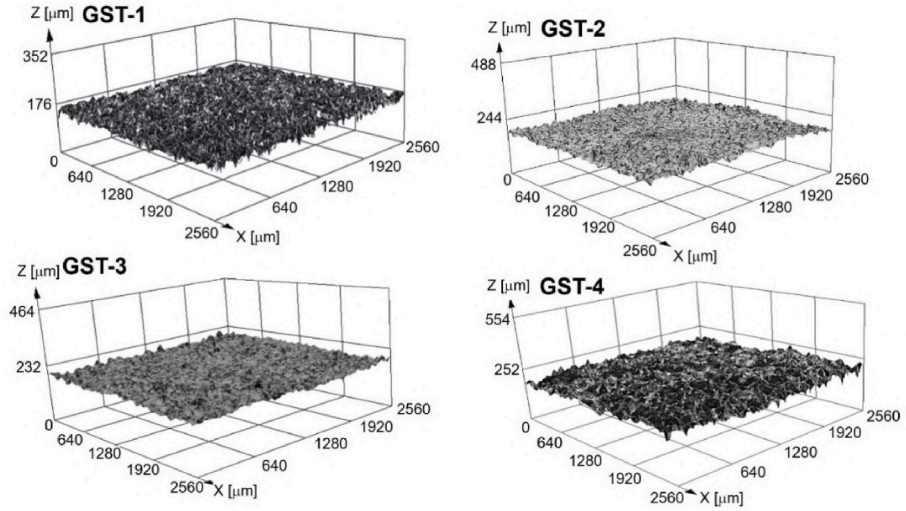

Fig. 6. 3D images of surface texture acquired on the surface of glazed PST.

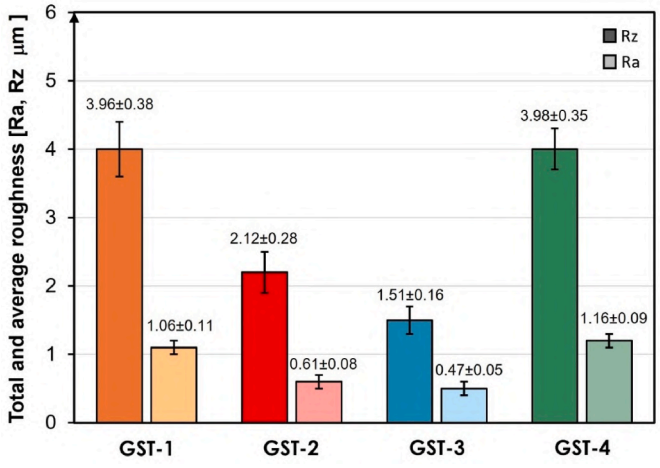

Fig. 7. Ra and Rz roughness parameters acquired on the glaze coating surface textures.

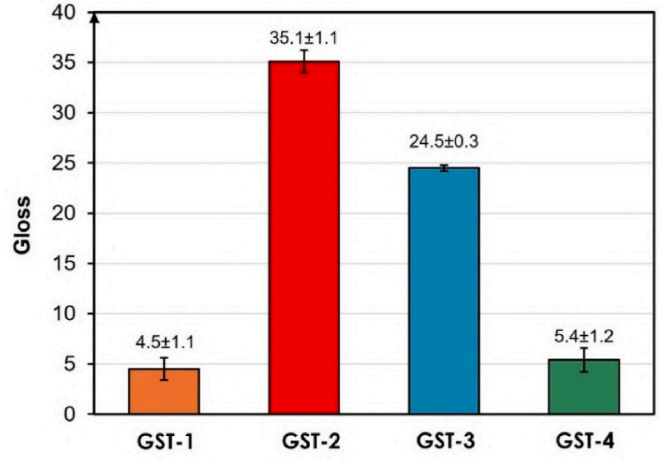

Fig. 8. Gloss values of the investigated glazes.

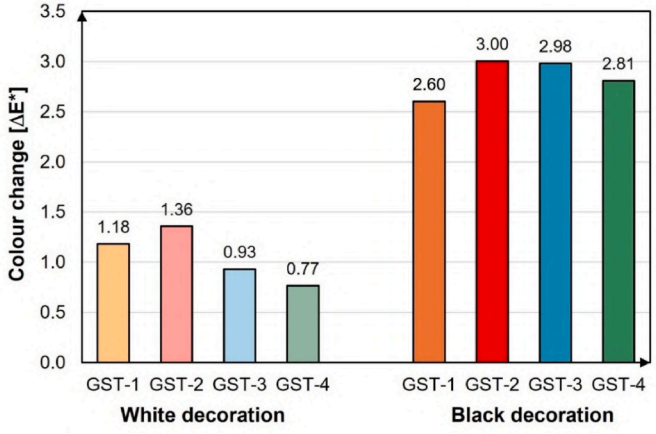

Fig. 9. Colour change (ΔE*) for GST-1, GST-2, GST-3 and GST-4 on full-colour white and full-colour black ceramic tiles. (For interpretation of the references to colour in this figure legend, the reader is referred to the Web version of this article.)

glaze application, and the corresponding ΔE* values are shown in Fig. 9. The ΔE* values obtained for full-coloured white ceramic tiles range from 0.77 to 1.36, indicating minimal variation, while the ΔE* values for full-coloured black tiles are slightly higher ($2.60 < \Delta E^* < 3.00$). In both cases, the original colours of decorations (white and black) are maintained, thus confirming that all the investigated glazes are fully transparent.

4. Conclusions

This study aimed to develop glass-ceramic glazes for porcelain stoneware tiles with low BaO content and a highly crystalline microstructure, to achieve high performance in terms of tribo-mechanical properties and aesthetic appearance. The main conclusions are as follows:

- microstructural investigations on GST-1, GST-3, and GST-4 reveal a microstructure predominantly consisting of a network of hyalophane ($K_{0.47}Ba_{0.4}Na_{0.13}Al_{1.41}Si_{2.6}O_8$) and Na-anorthite ($Ca_{0.54}Na_{0.48}Al_{1.52}Si_{2.48}O_8$) crystalline clusters. In contrast, GST-2 displays a microstructure primarily constituted by Na-anorthite, with sporadic

presence of (Ba, Na)-orthoclase ($Ba_{0.19}Na_{0.22}K_{0.59}Al_{1.18}Si_{2.82}O_8$) crystals;
- BaO concentration in glaze formulations significantly influences the type, size and amount of Ba-based crystalline phase, as well as glaze thermal behaviour. Specifically, in GST-1, GST-3, and GST-4, where BaO content is greater/equal to 2.5 mol%, the nucleation of hyalophane crystals is promoted. Moreover, in GST-1, the highest BaO concentration also increases glaze refractoriness and viscosity, inhibiting the growth of crystalline structures. This results in a finer microstructure and ultimately leads to incomplete densification. Conversely, in GST-2, where BaO concentration is equal to 1.1 mol%, the microstructure contains Na-anorthite and small amounts of (Ba, Na)-orthoclase;
- GST-4 is the most suitable glaze for the fast-firing cycle adopted in this study. The evaluation of its tribo-mechanical performances reveals the highest values for Vickers microhardness (HV = 8.9 ± 0.3 GPa), scratch resistance (SR = 7 Mohs) and surface roughness parameters (Ra = 1.16 ± 0.09 and Rz = 3.98 ± 0.35 μm). GST-4 performances are primarily attributed to the coexistence of hyalophane and Na-anorthite crystals in its microstructure, as well as trace amounts of BaO in the amorphous phase. The high crystalline content (64 wt%) also contributes to the low gloss value (5.4 ± 1.2), providing a desired matte appearance to the finished product.

The development of novel glass-ceramic glazes compatible with the firing cycle of porcelain stoneware tiles is of great relevance to the European ceramic industry, where this tile type accounts for over 70 % of the market. Glazes are key to ensuring both surface durability and aesthetic appeal, particularly as porcelain stoneware is increasingly used in diverse applications, including floor and wall coverings, furniture, and kitchen countertops. The addition of Ba in the tested amounts can be readily scaled up at the industrial level, and although incremental costs may vary by country, they are generally affordable to produce high-performance glazes. Indeed, continued research on glaze formulation is essential to tailor the required properties for durable and high-performance applications.

CRediT authorship contribution statement

Riccardo Fabris: Writing – original draft, Validation, Methodology, Investigation, Funding acquisition, Formal analysis, Data curation, Conceptualization. **Katarzyna Pasiut:** Writing – review & editing, Validation, Supervision, Methodology. **Giulia Masi:** Writing – review & editing, Visualization, Validation, Supervision, Methodology, Conceptualization. **Denia Mazzini:** Validation, Supervision, Resources, Methodology. **Giovanni Ridolfi:** Resources, Methodology. **Paweł Rutkowski:** Methodology, Investigation. **Janusz Partyka:** Supervision, Resources, Methodology. **Maria Chiara Bignozzi:** Writing – review & editing, Visualization, Validation, Supervision, Resources, Project administration, Funding acquisition, Conceptualization.

Declaration of competing interest

The authors declare that they have no known competing financial interests or personal relationships that could have appeared to influence the work reported in this paper.

Acknowledgements

Riccardo Fabris acknowledges the JECS Trust for funding a mobility stay project at the AGH University of Science and Technology, Krakow (Poland) in 2024 (Contract No. 2023376). Furthermore, the authors would like to acknowledge Fondazione Vittoriano Bitossi for funding the PhD grant. Carla Martini and Luca Lorenzetti (Department of Industrial Engineering, University of Bologna) are gratefully acknowledged for their valuable assistance with Vickers microhardness measurements.

References

[1] E. Sánchez, J. García-Ten, V. Sanz, A. Moreno, Porcelain tile: almost 30 years of steady scientific-technological evolution, Ceram. Int. 36 (2010) 831–845, https://doi.org/10.1016/j.ceramint.2009.11.016.
[2] S. Conte, C. Molinari, M. Ardit, G. Cruciani, M. Dondi, C. Zanelli, Porcelain versus porcelain stoneware: so close, So different. Sintering kinetics, phase evolution, and vitrification paths, Materials 16 (2023), https://doi.org/10.3390/ma16010171.
[3] M. Ambrosi, S. Santoni, R. Giorgi, E. Fratini, N. Toccafondi, P. Baglioni, High-performance and anti-stain coating for porcelain stoneware tiles based on nanostructured zirconium compounds, J. Colloid Interface Sci. 432 (2014) 117–127, https://doi.org/10.1016/j.jcis.2014.07.002.
[4] M. Romero, J.M. Pérez, Relation between the microstructure and technological properties of porcelain stoneware, Rev. Mater. Construt. 65 (2015), https://doi.org/10.3989/mc.2015.05915.
[5] R. Casasola, J.M. Rincón, M. Romero, Glass-ceramic glazes for ceramic tiles: a review, J. Mater. Sci. 47 (2012) 553–582, https://doi.org/10.1007/s10853-011-5981-y.
[6] A.M. Berto, Ceramic tiles: above and beyond traditional applications, J. Eur. Ceram. Soc. 27 (2007) 1607–1613, https://doi.org/10.1016/j.jeurceramsoc.2006.04.146.
[7] C. Zanelli, G. Baldi, M. Dondi, G. Ercolani, G. Guarini, M. Raimondo, Glass-ceramic frits for porcelain stoneware bodies: effects on sintering, phase composition and technological properties, Ceram. Int. 34 (2008) 455–465, https://doi.org/10.1016/j.ceramint.2006.11.008.
[8] J. Deubener, M. Allix, M.J. Davis, A. Duran, T. Höche, T. Honma, T. Komatsu, S. Krüger, I. Mitra, R. Müller, S. Nakane, M.J. Pascual, J.W.P. Schmelzer, E. D. Zanotto, S. Zhou, Updated definition of glass-ceramics, J. Non-Cryst. Solids 501 (2018) 3–10, https://doi.org/10.1016/j.jnoncrysol.2018.01.033.
[9] E.I. Cedillo-González, P. Chierici, M. Buttazzo, C. Siligardi, E. Blasi, A. Ardizzoni, Correlating the physico-chemical properties of two conventional glazed porcelain stoneware tiles in relation to cleanability and sanitization, Mater. Today Commun. 34 (2023), https://doi.org/10.1016/j.mtcomm.2022.105191.
[10] K. Kaczmarczyk, J. Partyka, K. Pasiut, J. Michałek, Strontium carbonate in glazes from the SiO_2–Al_2O_3–CaO–MgO–Na_2O–K_2O system, sintering and surface properties, Open Ceram. 9 (2022), https://doi.org/10.1016/j.oceram.2022.100233.
[11] R.A. Eppler, D.R. Eppler, Glazes and Glass Coatings, first ed., The American Ceramic Society, Westerville, Ohio, USA, 2000.
[12] L.J. Jaramillo Nieves, S. Nastri, A.V. Lot, F.G. Melchiades, G.A. Marsola, I. S. Flauzino, M.D.M. Innocentini, A.O. Boschi, Influence of engobe and glaze layers on the evolution of porosity and permeability of single-fired porcelain tiles, Appl. Clay Sci. 228 (2022), https://doi.org/10.1016/j.clay.2022.106635.
[13] F. Altindal, U.E. Anil, S.O. Varisli, B. Ozturk, Investigation of the effect of BaO-Al_2O_3 variations for BAS glass-ceramic glaze: insights into thermal, phase, microstructural and surface features, J. Eur. Ceram. Soc. 44 (2024) 3200–3209, https://doi.org/10.1016/j.jeurceramsoc.2023.12.073.
[14] R. Fabris, G. Masi, D. Mazzini, L. Sanseverino, M.C. Bignozzi, Tribomechanical properties of glazes for ceramic tiles: a novel protocol for their characterization, Materials 18 (2024) 60, https://doi.org/10.3390/ma18010060.
[15] R. Fabris, G. Masi, D. Mazzini, L. Sanseverino, M. Chiara Bignozzi, Application of different test methods to assess the wear resistance of ceramic tiles ceramic tile manufacture, in: Qualicer, Castellón De La Plana, 2024, p. 9. https://www.qualicer.org/programa/2024/ING/Ponencias/B/35%20paper%20ing.pdf.
[16] M. Gajek, A. Rapacz-Kmita, E. Stodolak-Zych, M. Zarzecka-Napierała, M. Wilk, A. Magdziarz, M. Dudek, Microstructure and mechanical properties of diopside and anorthite glazes with high abrasion resistance, Ceram. Int. 48 (2022) 6792–6798, https://doi.org/10.1016/j.ceramint.2021.11.230.
[17] S. Wang, X. Li, C. Wang, M. Bai, X. Zhou, X. Zhang, Y. Wang, Anorthite-based transparent glass-ceramic glaze for ceramic tiles: preparation and crystallization mechanism, J. Eur. Ceram. Soc. 42 (2022) 1132–1140, https://doi.org/10.1016/j.jeurceramsoc.2021.11.036.
[18] E. Barrachina, M. Esquinas, J. Llop, M.D. Notari, J.B. Carda, Development of a glass-ceramic glaze formulated from industrial residues to improve the mechanical properties of the porcelain stoneware tiles, Mater. Lett. 220 (2018) 226–228, https://doi.org/10.1016/j.matlet.2018.03.023.
[19] A.H.M. Hosseiny, A. Najafi, G. Khalaj, Investigation of CaO/MgO on the formation of Anorthite, Diopside, Wollastonite and Gehlenite phases in the fabrication of fast firing ceramic tiles, Constr. Build. Mater. 394 (2023), https://doi.org/10.1016/j.conbuildmat.2023.132022.
[20] M. Gajek, J. Partyka, A. Rapacz-Kmita, K. Gasek, Development of anorthite based white porcelain glaze without $ZrSiO_4$ content, Ceram. Int. 43 (2017) 1703–1709, https://doi.org/10.1016/j.ceramint.2016.08.140.
[21] S. Ke, X. Cheng, Y. Wang, Q. Wang, H. Wang, Dolomite, wollastonite and calcite as different CaO sources in anorthite-based porcelain, Ceram. Int. 39 (2013) 4953–4960, https://doi.org/10.1016/j.ceramint.2012.11.091.
[22] J. Partyka, K. Pasiut, P. Jeleń, J. Michałek, K. Kaczmarczyk, D. Kozień, The impact of nano-quartz on the structure of glass-ceramic glazes from the SiO_2–Al_2O_3–CaO–MgO–Na_2O–K_2O system, Ceram. Int. 46 (2020) 23888–23894, https://doi.org/10.1016/j.ceramint.2020.06.165.
[23] Z. Bao, S. Wang, L. Miao, Y. Xu, Z. Cheng, X. Wang, Preparation, properties and formation mechanism of transparent anorthite-based glass-ceramic glaze with high hardness, Ceram. Int. (2024), https://doi.org/10.1016/j.ceramint.2024.04.359.
[24] A. Tunali, E. Ozel, S. Turan, Production and characterisation of granulated frit to achieve anorthite based glass-ceramic glaze, J. Eur. Ceram. Soc. 35 (2015) 1089–1095, https://doi.org/10.1016/j.jeurceramsoc.2014.09.039.

[25] S. Banijamali, Preparation of glass-ceramic glazes for fast firing applications by CaF_2 substitution with B_2O_3 in the CaO–CaF_2–Al_2O_3–SiO_2 system, Ceram. Int. 39 (2013) 8815–8822, https://doi.org/10.1016/j.ceramint.2013.04.069.
[26] M. Gajek, M. Leśniak, M. Sitarz, E. Stodolak-Zych, A. Rapacz-Kmita, The crystallization and structure features of glass within the K_2O–MgO–CaO–Al_2O_3–SiO_2–(BaO) system, J. Mol. Struct. 1220 (2020), https://doi.org/10.1016/j.molstruc.2020.128747.
[27] J. Partyka, K. Gasek, K. Pasiut, M. Gajek, Effect of addition of BaO on sintering of glass–ceramic materials from SiO_2–Al_2O_3–Na_2O–K_2O–CaO/MgO system, J. Therm. Anal. Calorim. 125 (2016) 1095–1103, https://doi.org/10.1007/s10973-016-5462-2.
[28] J. Partyka, Effect of BaO addition on the structure and microstructure SiO_2–Al_2O_3–Na_2O–K_2O–MgO glass-ceramic composites, Ceram. Int. 41 (2015) 14013–14020, https://doi.org/10.1016/j.ceramint.2015.07.014.
[29] J. Partyka, Effect of BaO ratio on the structure of glass-ceramic composite materials from the SiO_2–Al_2O_3–Na_2O–K_2O–CaO system, Ceram. Int. 41 (2015) 9337–9343, https://doi.org/10.1016/j.ceramint.2015.03.282.
[30] M. Gajek, Study of the correlation between the composition, structure and crystallization in frits designed for single fast-firing glazes with variable BaO content, J. Therm. Anal. Calorim. 138 (2019) 4229–4236, https://doi.org/10.1007/s10973-019-08970-7.
[31] K. Pasiut, J. Partyka, D. Kozień, T. Kronberg, Impact of barium oxide on the structure and surface properties of glass-crystalline glazes, Ceram. Int. 50 (2024) 47980–47990, https://doi.org/10.1016/j.ceramint.2024.09.145.
[32] F.M. Stábile, M. Piccico, M.F. Serra, M. Rafti, G. Súarez, N.M. Rendtorff, Viscosity and thermal evolution of density and wetting angle of a commercial glaze by means of hot stage microscopy, Proc. Mater. Sci. 9 (2015) 563–570, https://doi.org/10.1016/j.mspro.2015.05.031.
[33] M.O. Prado, F.E. Benedetto, Assigning viscosity values in the glass softening temperature range, Materials 16 (2023), https://doi.org/10.3390/ma16041596.
[34] T. Kronberg, L. Hupa, Melting behaviour of raw glazes, J. Eur. Ceram. Soc. 39 (2019) 4404–4416, https://doi.org/10.1016/j.jeurceramsoc.2019.03.041.
[35] ASTM C1327-15, Standard Test Method for Vickers Indentation Hardness of Advanced Ceramics, American Society for Testing and Materials, 2019, 2019.
[36] ISO 6769, Vitreous and Porcelain Enamels – Determination of Surface Scratch Hardness According to the Mohs Scale, International Organization for Standardization, 2022.
[37] ISO 21920-2, Geometrical Product Specifications (GPS) – Surface Texture: Profile – Part 1: Indication of Surface Texture, International Organization for Standardization, 2022.
[38] W. Mokrzycki, M. Tatol, Color difference Delta E - a survey, machine graphics and vision 20, 383–411, https://www.researchgate.net/publication/236023905, 2011.
[39] S. Toyoda, S. Fujino, K. Morinaga, Density, viscosity and surface tension of 50RO-$50P_2O_5$ (R: Mg, Ca, Sr, Ba, and Zn) glass melts, J. Non-Cryst. Solids 321 (2003) 169–174, https://doi.org/10.1016/S0022-3093(03)00174-1.
[40] S.C. Whipkey, M.C. Modugno, H. Lee, W.M. Carty, Optimized etching of porcelain and polycrystalline alumina with a glass phase, J. Eur. Ceram. Soc. 41 (2021) 3761–3768, https://doi.org/10.1016/j.jeurceramsoc.2021.01.035.
[41] U. Täffner, V. Carle, U. Schäfer, M.J. Hoffmann, Preparation and microstructural analysis of high-performance ceramics, in: Metallography and Microstructures, ASM International, 2018, pp. 1057–1066, https://doi.org/10.31399/asm.hb.v09.a0003795.
[42] E.J. Essene, C.L. Claflin, G. Giorgetti, P.M. Mata, D.R. Peacor, P. ter Á rkai, M. A. Rathmell, Two-, three- and four-feldspar assemblages with hyalophane and celsian: implications for phase equilibria in $BaAl_2Si_2O_8$ – $CaAl_2Si_2O_8$–$NaAlSi_3O_8$–$KAlSi_3O_8$, Eur. J. Mineral 17 (2005) 515–535, https://doi.org/10.1127/0935-1221/2005/0017-0515.
[43] W. Liu, Z. Pang, J. Zheng, S. Yin, H. Zuo, The viscosity, crystallization behavior and glass-ceramics preparation of blast furnace slag: a review, Ceram. Int. 50 (2024) 18090–18104, https://doi.org/10.1016/j.ceramint.2024.02.374.
[44] J.L. Amorós, E. Blasco, A. Moreno, M.P. Gómez-Tena, C. Feliu, Non-isothermal sinter-crystallisation of satin glazes: a kinetic model, Ceram. Int. 44 (2018) 7780–7787, https://doi.org/10.1016/j.ceramint.2018.01.208.
[45] H.M.H. Zakaly, H.A. Saudi, S.A.M. Issa, M. Rashad, A.I. Elazaka, H.O. Tekin, Y. B. Saddeek, Alteration of optical, structural, mechanical durability and nuclear radiation attenuation properties of barium borosilicate glasses through BaO reinforcement: experimental and numerical analyses, Ceram. Int. 47 (2021) 5587–5596, https://doi.org/10.1016/j.ceramint.2020.10.143.
[46] M. Sheikhattar, H. Attar, S. Sharafi, W.M. Carty, Influence of surface crystallinity on the surface roughness of different ceramic glazes, Mater. Char. 118 (2016) 570–574, https://doi.org/10.1016/j.matchar.2016.07.003.